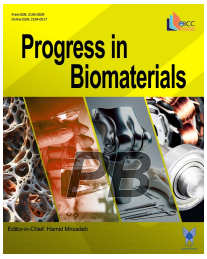

Volume 12, Issue 3, 122314 (1-13)

Progress in Biomaterials (PIBM)

https://doi.org/10.57647/pibm.2023.122314

Development of Thermal-Responsive Carboxymethylcellulose-Based Hydrogel Embedded with Fe-Based MOFs for Controlled Flutamide Release

Elham Rojouband[1], Saeid Mortazavinik[1], Mohammad Yousefi[2,*], Mandana Saber-Tehrani[1], Maryam Bikhof Torbati[3]

[1]*Department of Chemistry, NT.C., Islamic Azad University, Tehran, Iran.*
[2]*Department of Chemistry, TeMS.C., Islamic Azad University, Tehran, Iran.*
[3]*Department of Biology, YI.C., Islamic Azad University, Tehran, Iran.*

[*]**Corresponding author:** myousefi50@iau.ac.ir

Original Research

Received:
4 July 2023
Revised:
16 September 2023
Accepted:
20 September 2023
Published online:
30 September 2023

© 2023 The Author(s). Published by the OICC Press under the terms of the CC BY 4.0, Creative Commons Attribution License, which permits use, distribution and reproduction in any medium, provided the original work is properly cited.

Abstract:

This study investigates dual-functional drug delivery system utilizing Flutamide-loaded Fe_3O_4-doped Mil-100(Fe) nanoparticles embedded within a carboxymethyl cellulose (CMC) hydrogel, designed for magnetically triggered hyperthermia and controlled drug release. The synthesized NPs were integrated with CMC hydrogels. The final hydrogels were evaluated from the viewpoint of water uptake, porosity, degradation, cytotoxicity, drug release, and kinetic study. The Fe_3O_4-doped Mil-100(Fe) NPs exhibited higher drug loading capacity (26 ppm vs. 6 ppm) and enhanced porosity compared to unmodified NPs. CMC hydrogels incorporating these NPs displayed increased water uptake ($> 500\%$) and porosity, with Fe_3O_4-doped NPs showing a more significant impact. Degradation studies revealed similar trends for both NP-loaded hydrogels, although Fe_3O_4-doped NPs exhibited a slightly higher degradation rate (80%). MTT assays confirmed the biocompatibility of all hydrogel formulations, with cell viability exceeding 89%. Drug release studies, conducted under both physiological and alternating magnetic field (AMF) conditions, demonstrated Fickian diffusion kinetics for hydrogels. Fe_3O_4-doped NPs exhibited faster and more sustained Flutamide release, attributed to their higher loading capacity and porosity. AMF application slightly enhanced release rates, although the predominant control remained diffusion-limited. This work demonstrates the potential of Fe_3O_4-doped Mil-100(Fe) NPs within CMC hydrogels for targeted, magnetically triggered drug delivery and hyperthermia-based cancer therapy.

Keywords: Hydrogel; Drug delivery; Alternative magnetic field; Metal-organic framework; Cancer

Cite this article: Rojouband, E., Mortazavinik, S., Yousefi, M., Saber-Tehrani, M., Bikhof Torbati, M. Development of Thermal-Responsive Carboxymethylcellulose-Based Hydrogel Embedded with Fe-Based MOFs for Controlled Flutamide Release. *Progress in Biomaterials* **12**(1), Article 14 (2023).

1. Introduction

A non-invasive treatment method called alternative magnetic hyperthermia (AMH) uses magnetic fields to stimulate the body's natural healing processes. Despite being relatively recent in the treatment of cancer, clinical research has shown promising results. In the presence of magnetic nanoparticles (NPs), this method efficiently targets and destroys cancer cells by using the principle of magnetic hyperthermia, which involves applying a magnetic field to produce heat. A specialized applicator placed on the body's surface creates a magnetic field (Lemine, 2019). To improve targeting and therapeutic efficacy, this treatment uses tailored magnetic NPs, such as those that are encapsulated or functionalized with certain biomarkers. These NPs vibrate and produce localized heat when exposed to an alternating magnetic field (AMF), which raises the temperature in the tumor microenvironment. The high temperature, usually between 42 and 45 °C, causes necrosis and cellular apoptosis, which kills cancer cells alone while causing the least amount of harm to nearby healthy tissues (Lemine, 2019). Numerous studies have shown that a wide range of tumors,

including those of the breast, prostate, brain, and pancreas, can be treated with this targeted magnetic hyperthermia technique. It has also established itself as a promising option in contemporary cancer treatment due to its capacity for combination therapy, which can improve the results of immunotherapy, radiation, and chemotherapy (Gavilán et al., 2021).

On the one hand, creating and synthesizing magnetic NPs is essential to boosting the effectiveness of this treatment strategy. As a result, scientists are still looking for novel kinds of magnetic NPs for this treatment. The introduction of multifunctional magnetic NPs, which have additional functions besides raising the temperature, is a crucial strategy to boost the efficacy of this treatment. One of these impacts might be the release of a medication as the temperature rises (Olusegun et al., 2023). The combination of hydrogels and magnetic NPs offers a promising platform for hyperthermia treatment. MNPs are known for their superparamagnetic characteristics, which enable them to react to external magnetic fields (Hou et al., 2015). Typically, they are composed of materials like iron oxide. These NPs can improve the performance of hydrogels, which are three-dimensional networks of hydrophilic polymers, when they are placed within them. By using an AMF to create localized temperature increases, this combination enables the targeted and regulated release of medicines by remote heating (Uva et al., 2015). In addition to offering customizable mechanical characteristics and porosity for ideal drug loading and release profiles, the hydrogels offer a biocompatible environment that enhances the stability and efficacy of the MNPs.

A type of extremely porous material known as Metal-Organic Frameworks (MOFs) is made up of metal ions coupled to organic ligands, producing structures with tunable porosities and remarkably large surface areas (X. Chen et al., 2018). MOFs are appealing candidates for creating novel drug delivery systems because of their distinctive qualities. Researchers can use MOFs' high-loading capacity to encapsulate a range of medicinal substances, such as proteins, nucleic acids, and tiny compounds. Furthermore, controlled medication release is made possible by their porosity and pore diameters, which enable targeted and prolonged delivery to particular body locations (Zhao et al., 2022). The functionality of MOFs in drug delivery applications is further improved by modification. By adding different chemical groups to the MOF framework, researchers can improve loading efficiency and drug interaction (Cai et al., 2022; X.-X. Chen et al., 2021; Londoño et al., 2020). Targeting ligand functionalization allows for targeted administration to particular cells or tissues, boosting therapeutic effectiveness while reducing adverse effects. Modifications can also improve MOFs' stability and biocompatibility in physiological settings, which qualifies them for in vivo use. By improving these characteristics, researchers are opening the door to novel drug delivery systems that can react to outside stimuli (such as pH or temperature changes) and enhance therapeutic results in the management of a range of illnesses (Eshrati et al., 2022; Goli et al., 2021; Xue et al., 2018).

The walnut-sized prostate gland beneath the bladder is the site of prostate cancer, a common cancer in males that usually grows slowly and may go years without showing any symptoms. Surgery, radiation therapy, chemotherapy, cryotherapy, or hormone therapy are among the treatment options available, depending on the stage of the malignancy. In more advanced cases, the focus is primarily on symptom management. Because of its location, reaching the prostate frequently necessitates intricate procedures that include moving nearby organs (Schaeffer et al., 2023). Because of their special qualities and capacity to deliver therapeutic chemicals straight to the tumor site, injectable hydrogels offer a viable treatment option for prostate cancer (Ilgin et al., 2020; Norouzi et al., 2016). Due to their ease of injection, these biocompatible materials reduce the requirement for intricate surgical techniques that are frequently necessary to reach the prostate. Therapeutics can be released locally and continuously thanks to hydrogels' ability to swell after injection and create a gel-like matrix that surrounds medications. In addition to improving treatment efficacy, this tailored administration lowers systemic exposure and possible adverse effects. Researchers want to streamline the entire treatment procedure and enhance therapeutic outcomes in the management of prostate cancer by utilizing the benefits of injectable hydrogels (Ghandforoushan et al., 2023).

In this study, the main objective was to develop two types of magnetic NPs by modifying MOFs (MiL-100) with Fe ions that are targeted for flutamide delivery. This is the first time that the impact of doping Fe in the MiL-100 MOF has been studied regarding the release of Flutamide under magnetic fields. It was a question for us about how the modification of MOF by magnetic nanoparticles can affect the drug release. The NPs were integrated with carboxymethylcellulose (CMC) to develop an injectable hydrogel. As the main backbone of this study, the kinetics of Flutamide release were also studied.

2. Materials and methods

2.1 Chemicals

Iron (III) chloride and Trimesic acid (Merck, Germany) were purchased from local suppliers. Nitric acid and carboxymethylcellulose (CMC) were purchased from the Sigma-Aldrich supplier (USA). Flutamide was provided by NanoGolbarg Baharan Co. (Tehran, Iran). Phosphate buffer saline (PBS, Merck) was provided by a local supplier. Dimethyl sulfoxide (DMSO) and 3-(4,5-dimethyltiazole-2-yl)- 2,5-diphenyltetrazolium bromide (MTT) were purchased from Sigma–Aldrich (local supplier). HUVEC cell lines were purchased from the Pasteur Institute of Iran. All other chemicals were of reagent grade.

2.2 Synthesis of Mil-100 (Fe) NPs

First, 50 mL of deionized water was mixed with 3 g of iron (III) chloride and agitated for approximately an hour (solution A). Next, 50 mL of deionized water was mixed with 1.7 g of trimesic acid, and the mixture was agitated for two hours (solution B). 50 mL of deionized water (solution C) and 0.5 mL of nitric acid were combined in a different beaker. Subsequently, solutions A and B were concurrently added dropwise to solution C of nitric acid, and the mixture

was agitated for two hours. After that, the mixture was kept at 160 °C for 16 hours. The material was then collected after drying and filtered through Whatman filter paper (No. 42). For three hours, the sample precipitate was stored at 60 °C in 100 mL of 99.98% ethanol. Following that, the processes of filtration, washing, and sediment collecting were carried out. For six hours, the sample was kept at 50 °C in a vacuum oven.

2.3 Synthesis of Fe_3O_4@Mil-100(Fe) NPs

50 mL of deionized water (solution A) was mixed with three g of iron (III) chloride. Concurrently, 50 mL of deionized water (solution B) was mixed with 1.7 g of trimesic acid. Next, 50 mL of deionized water (solution C) was mixed with 0.5 mL of nitric acid and agitated. 10 mL of ethanol (solution D) and 0.6 g of nano iron oxide (Fe_3O_4) were combined in a different container and swirled for one hour. Solution D was then gradually supplemented with solution A. After that, it was mixed with solution B, which included trimesic acid. Following filtering, the sample was collected once it had dried. The material was stored at 60 °C in 100 milliliters of 99.98% ethanol for 3 h. Finally, the filtering, washing, and sediment collection steps were performed. The sample was placed in a vacuum oven at 50 °C for 6 h.

2.4 Synthesis of drug-loaded NPs

1 g of synthesized Mil-100(Fe) was added to 25 mL of flutamide drug solution with a concentration of 26 ppm and stirred for 24 hours. Then the solution was centrifuged, and the sample was dried (at room temperature for 24 h) and prepared for drug release. The same protocol was performed for Fe_3O_4@Mil-100(Fe) to prepare drug-loaded Fe_3O_4@Mil-100(Fe).

2.5 Drug loading efficiency

Samples from the Flutamide drug solution and the supernatant following centrifugation were taken during the manufacture of drug-loaded Fe_3O_4-Mil-100(Fe) and Mil-100(Fe) NPs. The Shimadzu UV-Vis spectrophotometer (model UV-160 A) was used to measure the amount of remaining flutamide.

2.6 Hydrogel synthesis

1 g of carboxymethyl cellulose was added to 50 mL of deionized water and stirred for 3 hours. Then, 0.01 g of Mil-100(Fe) powder containing flutamide was added and stirred for 12 hours. Next, 1 mL of 1% sodium polyphosphate TPP solution was added, and the final solution was stirred for 1 h. Then the sample was poured into a special plexiglass mold and placed in a freezer (−20) for 24 hours, and then freeze-dried for 40 h using (Dorsa freeze dryer (DRF-02 model, Iran). The same approach was performed to prepare hydrogels loaded with Fe_3O_4@Mil-100(Fe), Flut@Mil-100(Fe), and Flut@Fe_3O_4-Mil-100(Fe).

2.7 SEM and EDX

The morphology, and surface roughness of the NPs and hydrogels were examined using a scanning electron microscope (SEM, FEI Quanta 200) at an accelerating voltage of 25 kV. Before imaging, the sample surfaces were coated with a thin layer of gold, after which images were captured.

2.8 XRD Analysis

The crystallinity of the samples was assessed using X-ray diffraction (XRD, EQuniox 300, France) with Cu-Kα radiation. Measurements were performed over a 2θ range of $10-70°$ under operating conditions of 40 kV voltage and 30 mA current.

2.9 Swelling Behaviour

The method described in a previous study (Esmaeili et al., 2022) was adopted to evaluate the swelling behavior of the mats. Initially, the sample dry weight (w_0) was recorded. The hydrogels were then incubated in a 10 mM PBS solution (pH 7.4) at 37 °C. At specific time intervals, the hydrogels were removed, gently blotted with a Kimwipe to remove excess surface water, and weighed (w_t). The swelling ratio was determined using the following equation:

$$\%\text{Swelling} = \frac{w_t - w_0}{w_0} \times 100 \quad (1)$$

2.10 Degradation

The hydrogels were first weighed to record their initial mass (W_0). Subsequently, the samples were incubated in a 10 mM PBS solution (pH 7.4) at 37 °C for 1, 3, 5, 7, 9, 14, and 21 days to assess their degradation rate. At each time point, the PBS solution was removed, and the hydrogels were reweighed (W_t). The percentage of degradation was determined using the following formula (Qazi et al., 2022):

$$\%\text{Degradation} = \frac{W_0 - W_t}{W_0} \times 100 \quad (2)$$

2.11 Porosity

The porosity of hydrogels was evaluated using the liquid displacement method (Qazi et al., 2022). Ethanol was considered an alternative liquid because it rapidly enters the structure without dissolving or altering the structure of the wound dressing. To measure the porosity, 5 mL of ethanol was added to a 10 mL graduated cylinder (V_1). After that, the hydrogel samples were immersed in 96% pure ethanol for 30 minutes. After 30 minutes, the graduated cylinder's final, unaltered ethanol volume (V_2) was measured. After that, the hydrogels were removed from the ethanol such that there were no residues of the material left on their surface. The measured final volume of ethanol in the graduated cylinder is denoted by V_3.

$$P = \frac{V_1 - V_3}{V_2 - V_3} \times 100 \quad (3)$$

2.12 MTT assay

After being immersed in 70% ethanol for 24 hours, the hydrogel samples were disinfected for 1 hour under UV radiation (254 nm). After rinsing the hydrogels with sterile PBS, 4×105 HUVEC cells were added to each well of a 96-well plate. For twenty-four hours, the hydrogels were incubated at 37 °C with 5% CO_2. Following the incubation period, each well received 10 μL of MTT labeling reagent (0.5 mg/mL), and the plate was incubated for a further 4

hours. Following the addition of 100 μL of solubilization solution (DMSO) to each well, the plate was incubated for the entire night at 37 °C with 5% CO_2. Hydrogel-free cells were cultivated in different wells as a positive control. The formation of purple formazan crystals was observed, and the absorbance was measured at 570 nm using a Wareness Technology Microplate Reader. All experiments were conducted in triplicate (Manescu & P., 2021).

2.13 Drug release from hydrogels

The drug release from the hydrogel was conducted according to the following procedure (Esmaeili et al., 2023). Specifically, x mg of hydrogel was placed inside a dialysis bag, which was then submerged in 200 mL of distilled water and maintained under Conditions A and B. At predetermined time points (3, 9, 24, 42, 64, and 90 hours), 4 mL of the solution was withdrawn and replenished with an equal volume of fresh water.
Condition A: at 37 °C in an incubator without the Alternative Magnetic Field (AMF).
Condition B (S1): under AMF, according to the research done by Manescu et al. (Manescu & P., 2021) (S1). Briefly, the beaker containing the dialysis bag was located inside the coil, and the voltage and current were adjusted as follows: Voltage: 7 V, Current: 5 A. The beakers were exposed to the AMF every day for 20 min and then transferred to the incubator at 37 °C.
The AMF system description:

2.14 Release kinetic study

In this study, the release of numerical kinetic models was studied by considering the Korsmeier-Peppas model (Esmaeili et al., 2023).

$$F = \frac{Mt}{M\infty} = kt^n \tag{4}$$

where $Mt/M\infty$ represents the fraction of drug released at time t, k is the release rate constant, and n is the release exponent that indicates the mechanism of drug diffusion.

2.15 Statistical analysis

The data were analyzed using Prism software and ANOVA statistical tests. Results were presented as mean $\pm$ standard deviation, with a significance threshold set at $P < 0.05$.

3. Results and discussion

AMF technology utilizes oscillating magnetic fields to produce localized heating in magnetic NPs, which can be specifically targeted to cancerous tissues. Following systemic administration, the Fe-MOF NPs are designed to accumulate at the tumor site through passive or active targeting mechanisms. Once localized, applying an external AMF induces hyperthermia, raising the temperature within the tumor microenvironment. This controlled thermal effect enhances drug release from the Fe-MOF structure and follows the hydrogel while simultaneously inducing apoptosis and necrosis in cancer cells. By generating localized heating, this approach minimizes collateral damage to surrounding healthy tissues, thereby improving the therapeutic efficacy of Flutamide while reducing systemic side effects.
The primary objective of this study was to evaluate the feasibility of simultaneous drug delivery from MOF-loaded CMC hydrogel under AMF. This dual-functional approach aims to enhance cancer treatment by enabling targeted drug release while utilizing magnetic heating to induce localized hyperthermia, thereby improving therapeutic efficacy.
To achieve this, Mil-100(Fe) NPs were chosen as the base MOF due to their high surface area, tunable porosity, and biocompatibility, making them suitable candidates for drug loading and controlled release. The NPs underwent a two-step modification process to enhance their magnetic properties. First, they were functionalized with iron (Fe) to reinforce their structural stability and increase their responsiveness to external magnetic fields. Subsequently, Fe_3O_4 NPs were introduced to further improve their magnetic properties, enabling efficient heat generation when exposed to an alternating magnetic field (AMF). This modification resulted in the synthesis of two distinct nanostructures: Fe_3O_4-doped Mil-100(Fe) NPs (Fe_3O_4-Mil-100(Fe)) and unmodified Mil-100(Fe) NPs.
Following their synthesis, these MOF-based NPs were employed as drug carriers for Flutamide (Flut), a widely used anti-androgen drug for prostate cancer treatment. The drug was encapsulated within the porous structure of both nanoparticle formulations, leading to the formation of Flut@Fe_3O_4-Mil-100(Fe) (Flutamide-loaded Fe_3O_4-doped Mil-100(Fe)) and Flut@Mil-100(Fe) (Flutamide-loaded Mil-100(Fe)). Then, these NPs were loaded in CMC hydrogel.
Finally, the drug release profiles of the final hydrogels were investigated under standard physiological conditions and in the presence of an AMF environment. The primary goal was to determine how magnetic hyperthermia influenced the release kinetics of Flutamide from hydrogels. By leveraging magnetically induced heating, the study aimed to achieve an enhanced and more controlled drug release mechanism, thereby optimizing the therapeutic potential of Fe-based MOF NPs for cancer treatment.
Fig. 1 presents the SEM images of the synthesized NPs, both before and after Flutamide loading. The images include Mil-100(Fe) and Fe_3O_4-Mil-100(Fe) (without Flutamide) as well as Flut@Fe_3O_4-Mil-100(Fe) and Flut@Mil-100(Fe) NPs (with Flutamide encapsulation). As observed in Fig. 1, Mil-100(Fe) (Fig. 1 (a)) and Fe_3O_4-Mil-100(Fe) (Fig. 1 (b)) exhibit a multifaceted geometry, with sizes ranging from $60-200$ nm and $40-100$ nm, respectively. However, the synthesized Fe_3O_4-Mil-100(Fe) showed more uniform, smaller, and similar geometry than Mil-100(Fe). The reason is attributed to the presence of Fe_3O_4 within the structure. This size distribution is influenced by multiple factors, including reaction conditions, precursor concentration, pH of the reaction medium, and the balance between nucleation and growth. By optimizing these parameters, the particle size was successfully reduced from an initial 500 nm to below 200 nm, improving their suitability for biomedical applications. Additionally, the surface morphology appears smooth, lacking significant roughness or irregular features. In the case of Mil-100(Fe) NPs, a comparison before and af-

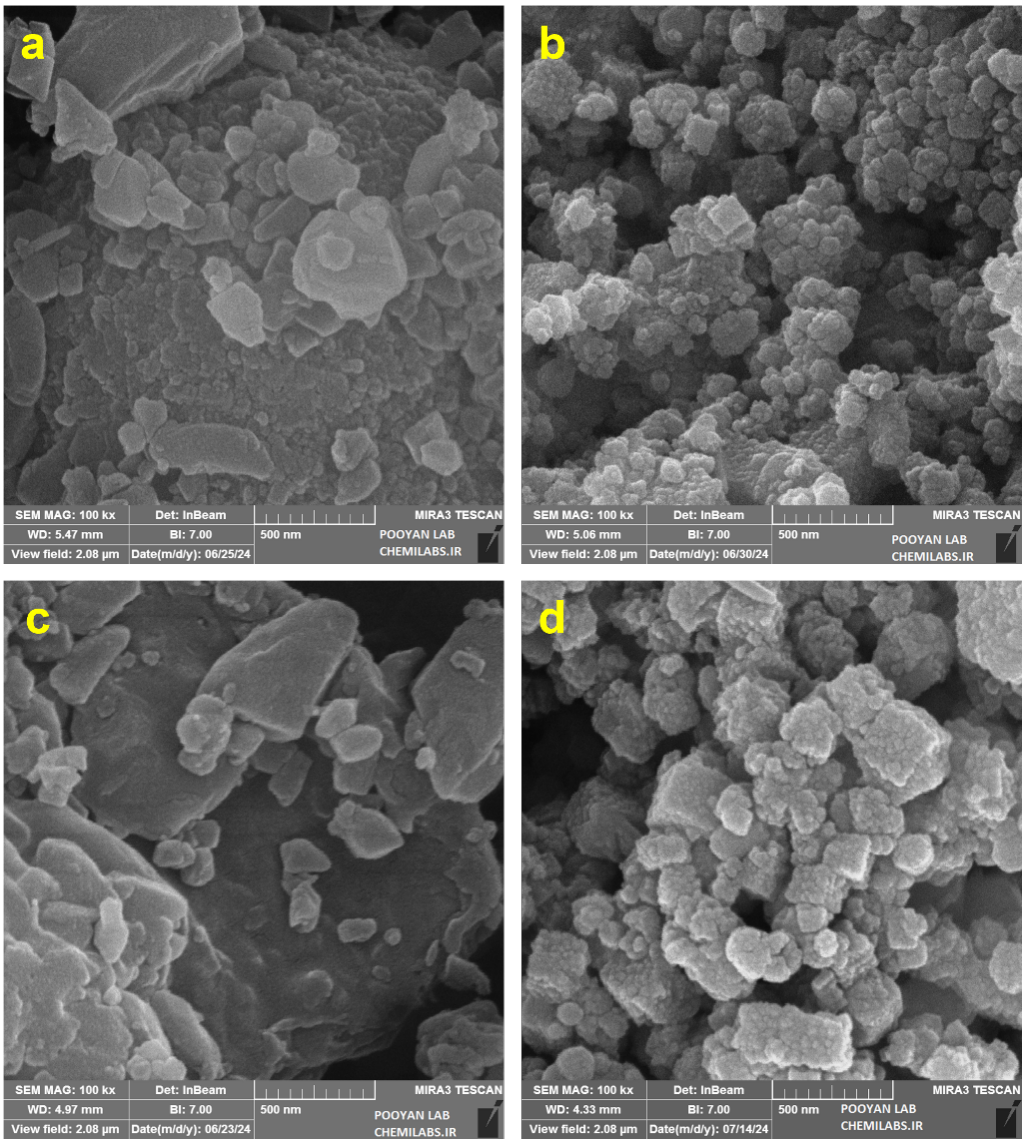

Figure 1. Results from SEM analysis for (a) Mil-100(Fe), (b) Flut@Mil-100(Fe) NPs and (c) Fe_3O_4-Mil-100(Fe) NPs, (d) Flut@Fe_3O_4-Mil-100(Fe) NPs.

ter Flutamide loading indicates that while the overall geometry of the NPs remained unchanged, a detectable increase in particle size was observed. This size enlargement is a well-documented phenomenon in MOF-based drug delivery systems, as the incorporation of drug molecules into the MOF framework often leads to structural modifications (X. Chen et al., 2018).

It has been reported that drug encapsulation within MOFs typically results in an increase in particle size due to the additional volume occupied by the loaded molecules. This expansion can be attributed to several factors, including the physical occupation of internal cavities, the formation of intermolecular interactions, and potential swelling effects within the porous structure (Champion et al., 2007). Additionally, the internal framework of the MOF may undergo conformational adjustments to accommodate drug molecules, which can influence the overall shape, crystallinity, and accessible surface area of the particles (Burtch et al., 2014). A similar effect was observed in the case of Mil-100(Fe), where structural reorganization likely contributed to the observed size increase.

Beyond changes in size, alterations in the crystal structure of MOF NPs can also occur upon drug loading. These modifications may involve pore expansion, variations in metal-ligand coordination angles, or even partial structural collapse due to the formation of new interactions between the drug molecules and the MOF backbone. Such alterations can significantly impact the porosity and surface area of the material, influencing its subsequent performance in biomedical applications, particularly drug release kinetics and adsorption efficiency.

Furthermore, chemical interactions between Flutamide and Mil-100(Fe), such as hydrogen bonding, $\pi - \pi$ stacking, and van der Waals forces, can play a crucial role in defining the stability, morphology, and functional properties of the loaded NPs. These interactions may affect drug loading capacity, release behavior, and overall bioavailability, making them critical factors in the design and optimization of MOF-based drug delivery systems (Wang et al., 2018).

In the case of Fe_3O_4-Mil-100(Fe) NPs, the synthesized

structures exhibited a multifaceted morphology, both before and after drug loading. However, unlike Mil-100(Fe) NPs, the Fe_3O_4-Mil-100(Fe) displayed a rough and rugged surface texture, which persisted even after Flutamide encapsulation. This distinct surface characteristic suggests that the Fe_3O_4 incorporation may have altered the external morphology of the MOF framework.

The diameter of the Fe_3O_4-Mil-100(Fe) NPs was measured within the range of $50 - 200$ nm, with a relatively narrow size distribution. Similar observations were reported by Aslam et al. (Aslam et al., 2017), where synthesized Fe_3O_4-Mil-100(Fe) NPs exhibited a rough surface and a size distribution between 73.5 and 148 nm. Their study also confirmed that dye loading did not significantly alter the geometry or surface roughness of the NPs, indicating that the porous structure of MOFs can accommodate guest molecules without disrupting their external morphology.

Furthermore, a comparison between Fe_3O_4-Mil-100(Fe) and Flut@Fe_3O_4-Mil-100(Fe) NPs suggests that Flutamide loading occurred primarily through entrapment within the MOF's porous network, rather than surface adsorption. The ability of MOFs to encapsulate drug molecules within their internal cavities while maintaining their external morphology is a crucial feature that enhances their drug delivery efficiency, stability, and controlled release behavior (Zheng et al., 2016). The presence of Fe_3O_4 NPs within the system may also contribute to enhanced magnetic targeting capabilities, further improving the potential of these materials for stimuli-responsive drug delivery and hyperthermia-based cancer therapy (Manescu & P., 2021).

Fig. 2 (a), 2 (b) and Fig. 2 (c), (d) present the microscopic structure of Mil-100(Fe)-loaded CMC and Fe_3O_4-doped Mil-100(Fe)-loaded CMC hydrogels, respectively. The SEM micrographs reveal that the inner surface of the hydrogels exhibits a rough and highly porous morphology, with NPs distributed randomly throughout the structure.

In figure 2(a) and figure 2(c), lower magnification images illustrate the overall porous network of the hydrogel matrices, highlighting their heterogeneous and interconnected nature. The incorporation of Mil-100(Fe) and Fe_3O_4-doped

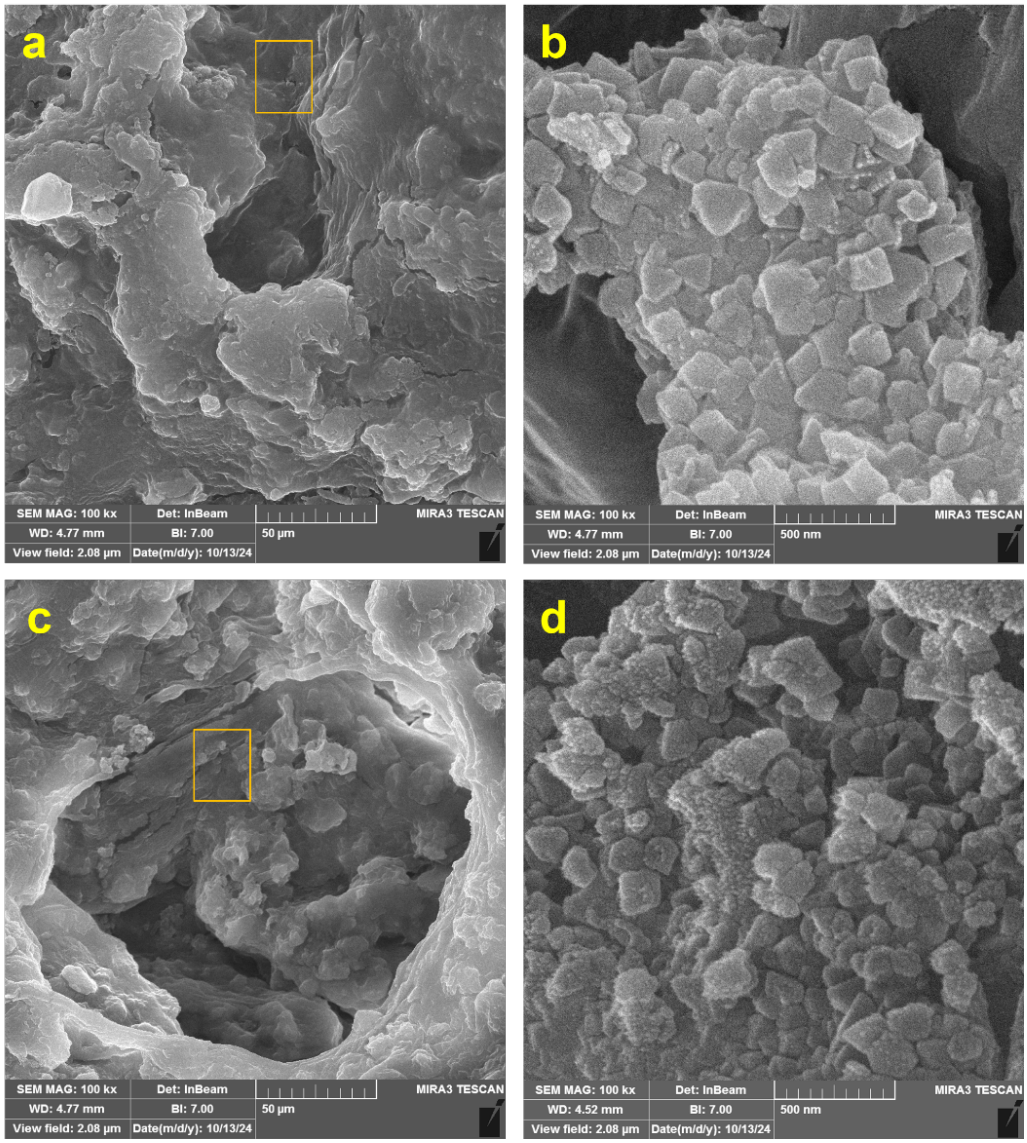

Figure 2. Results from SEM analysis for CMC hydrogel integrated with (a), (b) Mil-100(Fe) NPs and (c), (d) Fe_3O_4-Mil-100(Fe) NPs.

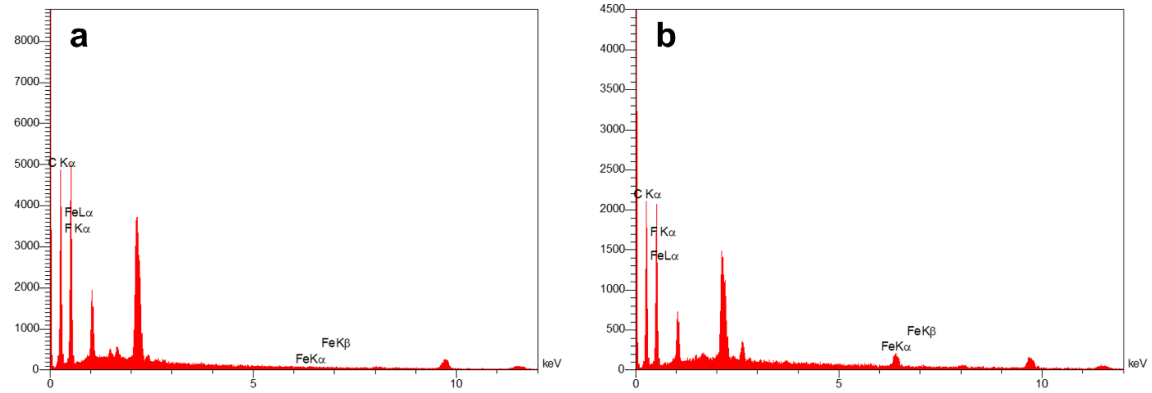

Figure 3. EDX analysis for CMC hydrogel integrated with (a) Flut@Mil-100(Fe) NPs and (b) Flut@Fe_3O_4-Mil-100(Fe) NPs.

Mil-100(Fe) NPs results in an evident modification of the surface roughness and porosity. Meanwhile, figure 2(b) and figure 2(d), which provide higher magnification views, further emphasize the dense accumulation of NPs on the hydrogel surface.

Fig. 3 demonstrates the proof of Fe existence in the hydrogels which confirms the presence of Mil-100(Fe) and Fe_3O_4-doped Mil-100(Fe) NPs. According to the results, both groups showed the presence of Fe atoms. The Fe content was higher for CMC hydrogel loaded with Fe_3O_4-doped Mil-100(Fe) rather than that with Mil-100(Fe), which the reason turns back to Fe_3O_4. The presence of the "F" atom confirmed the presence of Flutamide because F is one of the main atoms in its structure (Karthik et al., 2017).

Regarding the ability of NPs for Flutamid loading, Mil-100(Fe) and Fe_3O_4-Mil-100(Fe) NPs could load 6 ppm and 26 ppm of Flutamide, respectively. The main reason for this difference can be attributed to the presence of Fe_3O_4 in the structure of Mil-100(Fe), which caused more porosity. It can be claimed that doping Fe_3O_4 to the MIL-100(Fe) structure has significant effects on the physical and chemical properties of the MIL-100 (Fe) NPs, especially its porosity, which is a critical point for drug delivery systems. Fe_3O_4, which is known as a magnetic nanoparticle, can change the pore structure and surface area of this metal-organic framework when combined with MIL-100 (Fe), depending on its bonding.

Fig. 4 depicts the results from XRD analysis which indicates the crystalline properties of CMC hydrogels loaded with Flut@Mil-100(Fe) and Flut@Fe_3O_4-Mil-100(Fe). Fig. 4 (a) shows that Flut@Mil-100(Fe)-CMC hydrogels own a low crystallinity indicated by a wide peak at $2\theta = 22°$ and a small sharp peak at $2\theta = 12°$ that was attributed to the presence of Mil-100(Fe). In contrast, CMC hydrogel loaded with Flut@Fe_3O_4-Mil-100(Fe) showed higher crystallinity by showing a large, sharp peak at $2\theta = 12°$ and some small, sharp peaks in the range of $2\theta = 20 - 30°$. These changes in the crystallinity were justified by the presence of Fe_3O_4 within the structure of Mil-100(Fe) (Sun et al., 2017).

Based on the previous studies, CMC, in their pure form (free of drugs, NPs, or other additives), generally exhibit a semi-crystalline structure (Tuan et al., 2021). The degree of crystallinity in CMC depends on factors such as the degree of substitution (DS) of the carboxymethyl groups, the moisture content, and the preparation conditions. CMC itself is derived from cellulose, a natural polymer with crystalline regions. However, during the carboxymethylation process, the cellulose's crystalline structure is partially disrupted, leading to an amorphous nature in CMC. The degree of crystallinity in CMC hydrogels is typically low, as the hy-

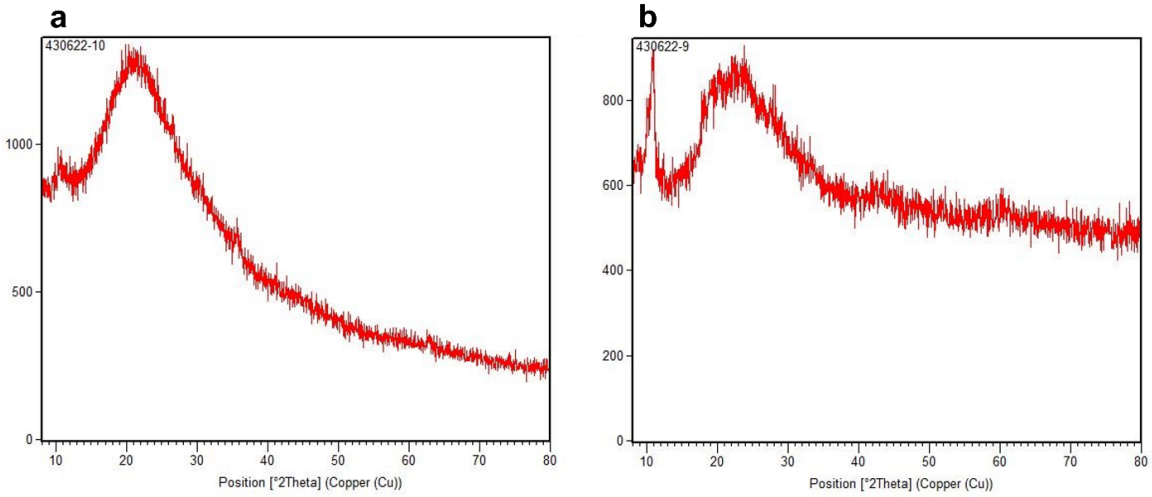

Figure 4. XRD analysis for CMC hydrogel integrated with (a) Flut@Mil-100(Fe) NPs and (b) Flut@Fe_3O_4-Mil-100(Fe) NPs.

drophilic nature of the carboxymethyl groups causes the polymer chains to become more flexible and disordered when in contact with water (El-Lateef et al., 2020). The presence of water in CMC hydrogels further reduces the crystallinity because water acts as a plasticizer, causing the polymer chains to swell and adopt a more amorphous, hydrated structure. The water content can therefore influence the overall crystallinity of the hydrogel, as the polymer chains are less ordered in the swollen state (Casaburi et al., 2018).

Fig. 5 (a) shows the results of hydrogel behavior from the viewpoint of water uptake. As can be seen, the addition of Flut@Mil-100(Fe) NPs to the CMC hydrogel showed an increase in water uptake but not significantly ($P > 0.05$). It can be concluded that by incorporating more Flut@Mil-100(Fe) NPs with hydrogel, a significant difference can be achieved. More interestingly, by adding the same amount of Flut@Fe_3O_4-Mil-100(Fe) NPs, a significant ($P < 0.01$) difference in water uptake was observed for CMC.

Fig. 5 shows the results of hydrogel behavior from the viewpoint of water uptake. As can be seen, the addition of Flut@Mil-100(Fe) NPs to the CMC hydrogel showed an increase in water uptake but not significantly ($P > 0.05$) (around 400% to 500%). This behavior can be attributed to the fact that Flut@Mil-100(Fe) NPs, despite their potential to increase the surface area and interaction sites within the hydrogel network, may not be sufficiently hydrophilic or might not interact strongly enough with the CMC chains to induce a notable change in water retention. The increase in water uptake is likely due to a slight increase in the porosity or the ability of the hydrogel to form more hydrogen bonds with water molecules, but this effect may not be drastic enough to yield statistically significant results at the given concentration (Tuan et al., 2021).

It can be concluded that by incorporating more Flut@Mil-100(Fe) NPs with the hydrogel, a significant difference could be achieved. This suggests that a higher concentration of Flut@Mil-100(Fe) NPs could increase the interstitial spaces or provide additional hydrophilic sites, promoting enhanced water absorption. Furthermore, higher NP concentrations could also facilitate improved interaction between the NPs and the CMC matrix, leading to more pronounced water uptake (Tuan et al., 2021).

More interestingly, by adding the same amount of Flut@Fe_3O_4-Mil-100(Fe) NPs, a significant ($P < 0.01$) difference in water uptake was observed for CMC (around 400% to 600%). The enhanced water uptake observed can be attributed to several factors. First, Flut@Fe_3O_4-Mil-100(Fe) NPs are known to possess a magnetic property that could influence the hydrogel's structure at the nanoscale level (Hamidian & Tavakoli, 2016). The presence of magnetic Flut@Fe_3O_4-Mil-100(Fe) NPs may induce an alignment or reorganization of CMC chains, potentially leading to better hydration and swelling behavior. Additionally, these NPs can enhance the surface energy of the hydrogel, promoting stronger interactions with water molecules. This interaction may result in more efficient water retention, as the surface of the nanoparticles could provide additional hydrophilic sites, which aid in the absorption and retention of water. Moreover, magnetic particles may also influence the overall network structure, causing changes in crosslinking density or porosity that are favorable for water uptake (Ebrahimi & Bardajee, 2021). These factors, combined with the potential synergistic effects between Fe_3O_4 and Mil-100(Fe), contribute to the observed significant increase in water uptake ($P < 0.01$) compared to the Flut@Mil-100(Fe) NPs.

Regarding porosity, Fig. 5 (b) shows the impact of NPs on the porosity of CMC hydrogel. As can be seen, the integration of both types of NPs with the CMC hydrogels caused a significant difference compared to the simple CMC hydrogel ($P < 0.05$). This finding suggests that the incorporation of nanoparticles into the hydrogel matrix has a noticeable effect on the overall structural characteristics, particularly in terms of pore formation and size distribution. The increase in porosity can be attributed to the introduction of nanoparticles, which likely disrupt the uniformity of the CMC network, creating additional void spaces within the hydrogel structure (Wu et al., 2022).

The incorporation of NPs such as Flut@Mil-100(Fe) and Flut@Fe_3O_4-Mil-100(Fe) NPs into CMC hydrogels can result in the formation of interstitial gaps between polymer chains, thereby increasing the pore volume. This effect is due to the physical presence of nanoparticles acting as filler materials that may not entirely integrate into the polymeric network but instead create spaces that can enhance porosity (Campea et al., 2021). The surface characteristics of these nanoparticles can also influence the hydrogel's morphology by promoting the formation of larger pores or channels as the nanoparticles aggregate or interact with CMC chains. Additionally, the compatibility and interaction between CMC and the nanoparticles might influence the extent of porosity enhancement (He et al., 2009).

This issue confirms that the distribution of both types of nanoparticles within the structure of the CMC hydrogel caused a similar impact. Despite differences in their composition, both Flut@Mil-100(Fe) and Flut@Fe_3O_4-Mil-100(Fe) NPs appear to affect the hydrogel matrix comparably, likely by inducing a similar degree of disruption in the hydrogel network. This suggests that the nature of the nanoparticles, whether functionalized with Flutamide or doped with Fe_3O_4, does not significantly alter their ability to modify the structural integrity of the hydrogel in terms of porosity. The uniformity of nanoparticle distribution within the hydrogel and their interactions with the CMC chains may play a key role in determining the extent of the observed porosity changes.

The impact of water uptake and porosity can be directly linked to the degradation behavior of the hydrogels. Fig. 5 (c) presents the degradation results over 21 days. As observed, the pure CMC hydrogel exhibited the lowest degradation rate throughout the entire period. This behavior can be attributed to the intrinsic stability of the CMC hydrogel network, where the absence of nanoparticles results in a more compact and less porous structure, reducing its susceptibility to hydrolytic degradation. Since degradation in hydrogels is often governed by water diffusion and polymer chain cleavage, the lower water uptake and reduced porosity

of pure CMC likely contribute to its slower degradation profile (Olad et al., 2018).

Interestingly, both Flut@Mil-100(Fe)-loaded hydrogel and Flut@Fe_3O_4-Mil-100(Fe) -loaded hydrogel exhibited a similar degradation trend, with no significant difference in their degradation rates (> 80%). This suggests that while the incorporation of nanoparticles influences structural parameters such as porosity and water uptake, it does not drastically alter the degradation kinetics under the tested conditions. One possible explanation is that both types of nanoparticles are well integrated into the hydrogel matrix, preventing rapid structural disintegration while still allowing a gradual breakdown (Sethi et al., 2019).

However, a higher degradation rate was recorded for the Flut@Fe_3O_4-Mil-100(Fe) -loaded hydrogel. This increased degradation may be attributed to several factors. First, the enhanced water uptake observed in this hydrogel likely accelerates hydrolytic degradation, as a greater influx of water facilitates polymer chain cleavage and hydrogel disintegration (Thang et al., 2023). Second, the Flut@Fe_3O_4-Mil-100(Fe) NPs might induce localized structural changes within the hydrogel matrix, potentially weakening the polymer-nanoparticle interactions and allowing faster degradation. Moreover, the presence of Flut@Fe_3O_4-Mil-100(Fe) NPs could influence hydrogel network stability by modifying crosslinking density or introducing additional hydrophilic sites that further enhance degradation (Li et al., 2012).

Overall, these results demonstrate how water absorption, porosity, and NP composition are interrelated factors that affect how CMC-based hydrogels degrade. While nanoparticle incorporation alters hydrogel properties, its effect on degradation depends on the extent of water absorption and the structural modifications induced by the nanomaterials.

The absence of cytotoxicity in both hydrogels and incorporated NPs is a crucial biological consideration that must be thoroughly evaluated, especially for biomedical applications (Shah et al., 2016). Since hydrogels serve as carriers for bioactive agents, their interaction with cells and tissues must not trigger adverse effects, such as inflamma-

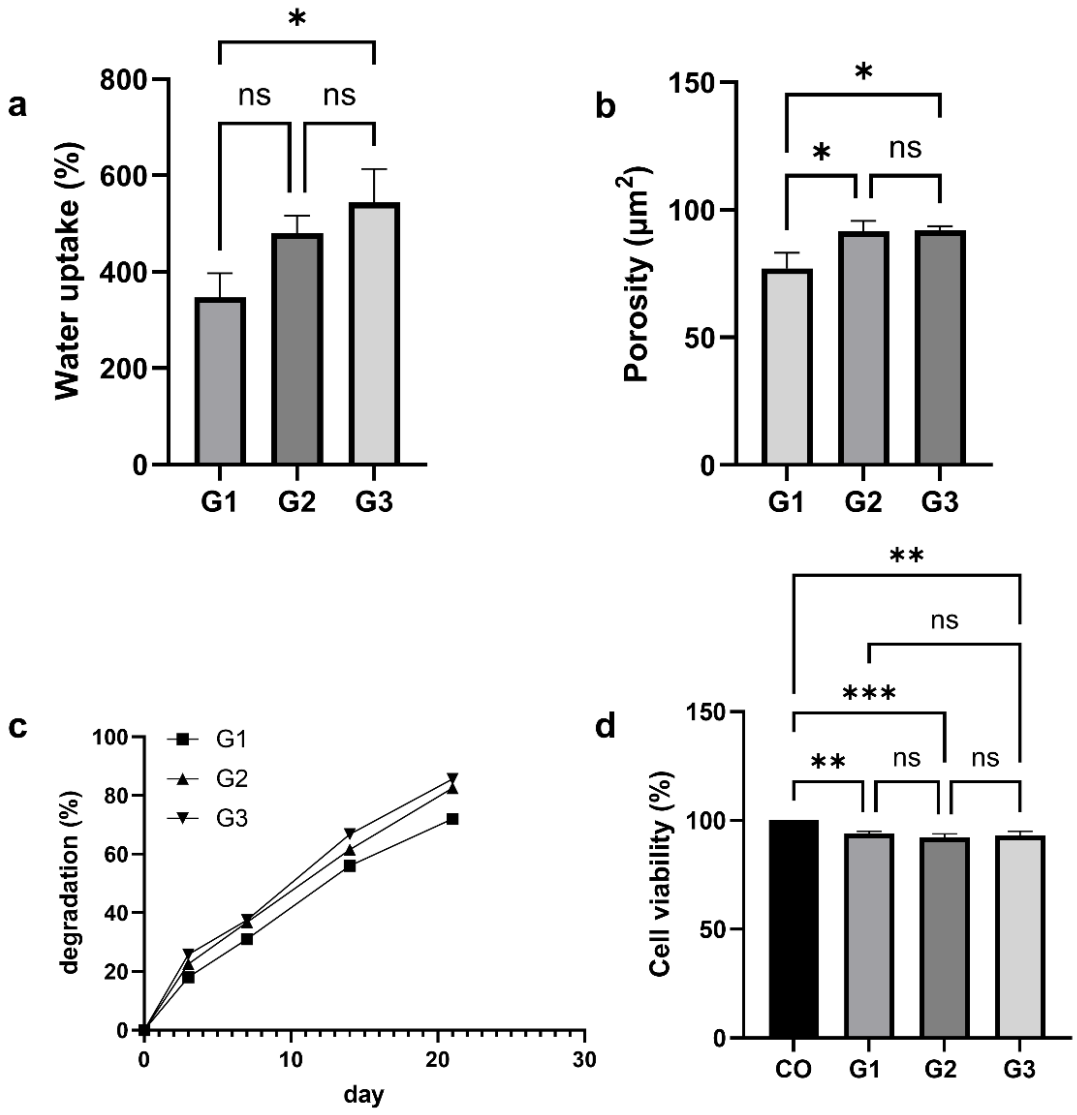

Figure 5. Results from (a) Water uptake analysis, (b) Porosity, (c) Degradation, (d) Cell viability after 24h, for G1(CMC hydrogel), G2 (Flut@Mil-100(Fe)-loaded hydrogel), and G3 (Flut@Fe_3O_4-Mil-100(Fe) -loaded hydrogel).

tion, apoptosis, or impaired cell viability. In this study, ensuring the biocompatibility of CMC-based hydrogels and their NP-loaded variants is particularly important, as any toxic response could compromise their intended function in controlled Flutamide release. Given that Flut@Fe_3O_4-Mil-100(Fe) and Flut@Mil-100(Fe) NPs have been incorporated into the hydrogel matrix, it is essential to assess whether their presence alters cell viability or induces any cytotoxic effects over time.

Fig. 5 (d) presents the MTT assay results, evaluating the cytotoxicity of the synthesized hydrogels after 24 hours of exposure to HUVEC cells. As shown, the control group (without hydrogel exposure) maintained 100% cell viability, serving as the baseline reference. The CMC hydrogel exhibited a cell viability of 99%, while Flut@Mil-100(Fe)-loaded CMC hydrogel and Flut@Fe_3O_4-Mil-100(Fe)-loaded CMC hydrogel demonstrated viabilities of 93% and 89%, respectively. Although the nanoparticle-loaded hydrogels showed slightly reduced cell viability compared to the pure CMC hydrogel, the differences among the hydrogel groups were not statistically significant ($P > 0.05$), indicating that the incorporation of nanoparticles did not induce substantial cytotoxic effects. Notably, all hydrogel formulations maintained high cell viability ($> 89\%$), further confirming their biocompatibility. Despite a statistically significant reduction in viability compared to the control group, the observed values still fall within an acceptable range for biomaterials intended for biomedical applications.

When compared with previous studies on CMC-based hydrogels, the results are consistent with findings that CMC itself is inherently biocompatible and does not significantly impair cell proliferation (Reza & Nicoll, 2010). Studies have shown that unmodified CMC hydrogels typically support cell viability above 95%, making them suitable for tissue engineering and drug delivery applications (Pourmadadi et al., 2023). However, variations in viability can occur depending on the type and concentration of incorporated NPs. For example, previous studies incorporating MOFs into CMC hydrogels have reported minor reductions in cell viability, likely due to the initial burst release of encapsulated compounds or potential oxidative stress from nanoparticle interactions (Javanbakht et al., 2019). In this study, the slightly lower viability of the Flut@Fe_3O_4-Mil-100(Fe)-loaded hydrogel compared to the Flut@Mil-100(Fe)-loaded hydrogel suggests that the presence of Fe_3O_4 may introduce mild cellular stress, potentially due to its magnetic properties or surface interactions. However, given that viability remained above 89%, the results confirm that these hydrogels are non-toxic and suitable for biomedical applications, particularly in sustained drug delivery and tissue engineering, where prolonged exposure to biomaterials is expected. Furthermore, the impact of NPs on hydrogel behavior, such as water uptake, porosity, and degradation, could also influence their biological safety (Javanbakht et al., 2019). A higher porosity and water uptake may enhance cell-nutrient exchange, but excessive degradation could lead to the uncontrolled release of nanoparticles, which may have unintended interactions with biological systems. Additionally, the prolonged release of Flutamide from the hydrogel must be monitored to prevent local toxicity at the site of application (Smagina et al., 2023).

Fig. 6 shows the outcomes of Flutamide release from NPs-loaded CMC hydrogels under both normal and AMF conditions. The results of the kinetic analysis employing the

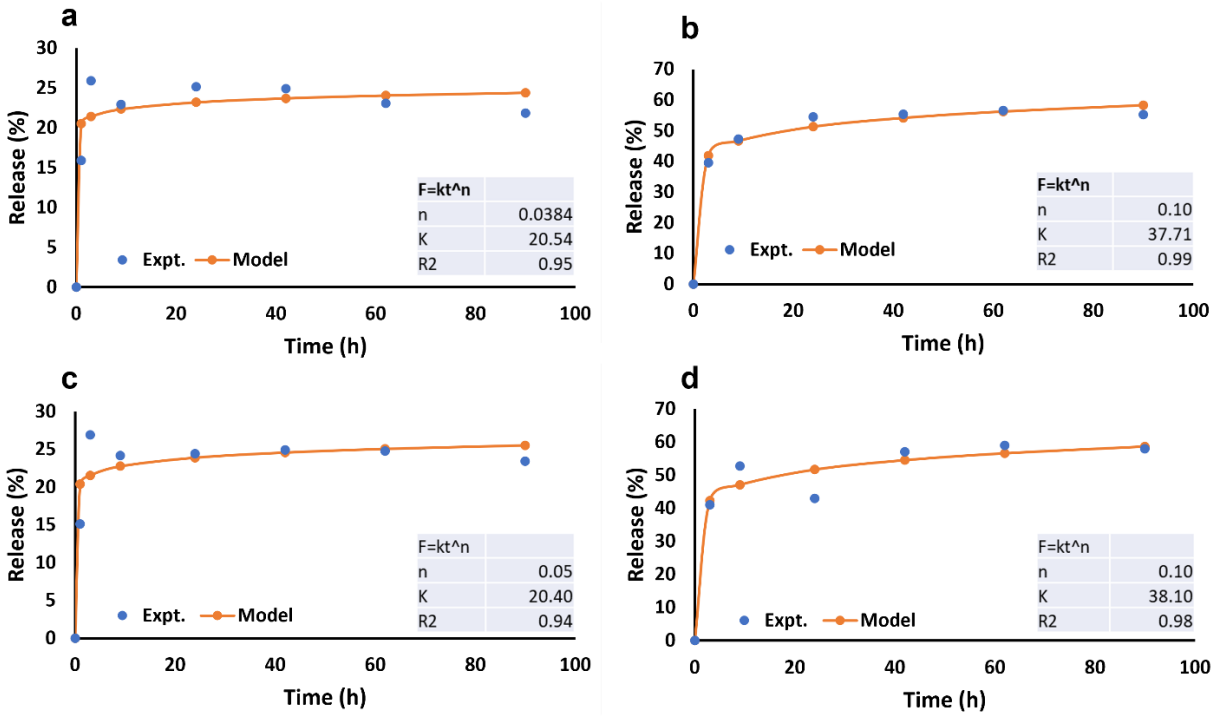

Figure 6. Drug release from Np-loaded hydrogels. (a) CMC hydrogel integrated with Flut@Mil-100(Fe) NPs without AMF, (b) Hydrogel integrated with Flut@Fe_3O_4-Mil-100(Fe) NPs without AMF, (c) Hydrogel integrated with Flut@Mil-100(Fe) NPs under AMF, (d) Hydrogel integrated with Flut@Fe_3O_4-doppedMil-100(Fe) NPs under AMF.

"Korsmeyer-Peppas model," one of the most well-known models for analyzing release rate including the power of "n" and the constant coefficient of "k", is also shown in Fig.Fig. 6. The value of "n" helps classify the release mechanism, such as Fickian diffusion ($n \leq 0.5$), non-Fickian or anomalous transport ($0.5 < n < 1$), and case-II transport ($n \geq 1$) (Esmaeili et al., 2023).

Without AMF: According to Fig. 6 (a), which shows the release results for CMC hydrogel integrated with Flut@Mil-100(Fe), a fast release of about 20% was observed after 3 h. After 90 h of release, about 25% of the loaded Flutamide was released gradually. It seems that a fast release was observed during the first hours. However, considering the same experiment for Flut@Fe_3O_4-Mil-100(Fe) -loaded CMC hydrogel (Fig. 6 (b)), it can be claimed that about 39% of the loaded Flutamide was released after 3 h, and the release enhanced to about 50% after 90 h. By considering the results from the kinetic study, it can be concluded that in both groups, the release kinetic is governed by Fickian diffusion ($n = 0.038$ and 0.1, $n < 0.5$). The coefficient k increased from 20.54 to 37.71, which confirms a faster diffusion. This issue can be attributed to the more drug releases from Flut@Fe_3O_4-Mil-100(Fe) due to higher Flutamide loading.

Under AMF: Fig. 6 (c) and Fig. 6 (d) show the results of Flutamide release from Flut@Mil-100(Fe)-loaded CMC hydrogel and Flut@Fe_3O_4-Mil-100(Fe) -loaded CMC hydrogel under AMF conditions, respectively. According to Fig. 6 (c), after 3 h, about 28% of Flutamide was released from CMC hydrogel. By prolonging the release process, no significant increase was observed in the Flutamide release. Regarding Fig. 6 (d), 41% of Flutamide was released during the first 3 hours of the study, and after 90 hours, the release ratio increased to about 60%. Considering the release kinetics, both groups showed that the release kinetics is governed by Fickian diffusion ($n = 0.05$ and 0.1, $n < 0.5$). The coefficient k increased from 20.40 to 38.1, which confirms a faster diffusion. This issue can be attributed to the more drug releases from Flut@Fe_3O_4-Mil-100(Fe) due to higher Flutamide loading.

As a result of the kinetic study, it can be claimed that the presence of Fe_3O_4 in the Mil-100(Fe) NPs affects the release of Flutamide under AMF. In a part of our study, we confirmed this issue (data not provided). The released drug is still entrapped in the hydrogel structure. It means that release from the hydrogel can control the final release rate. It can also be concluded that the presence of AMF did not affect the Flutamide release from CMC hydrogel (Esmaeili et al., 2023).

It was hypothesized that Fe_3O_4-doped Mil-100(Fe), due to its higher porosity, would have a greater capacity to encapsulate Flutamide within its porous network (Bhattacharjee et al., 2020). The increased surface area and interconnected pore structure provide more binding sites, allowing for a higher drug-loading efficiency. Consequently, the diffusion of Flutamide from these porous structures is expected to occur over an extended period, resulting in a more sustained and controlled release profile.

In contrast, Mil-100(Fe), as indicated by SEM analysis, appears to have a lower porosity. This reduced porosity limits the available space for drug entrapment, leading to a lower Flutamide loading capacity. Additionally, in less porous structures, the drug molecules are more likely to be adsorbed near the surface rather than being deeply embedded within the matrix. As a result, Flutamide is released more rapidly, following a burst-like release pattern. In general, a lower porosity facilitates faster drug diffusion due to shorter diffusion pathways and weaker entrapment within the material.

4. Conclusion and future perspectives

This study successfully developed and characterized a new drug delivery system based on Fe_3O_4-doped Mil-100(Fe) NPs embedded in a CMC hydrogel for the controlled release of Flutamide, with potential application in magnetic hyperthermia-assisted cancer therapy. The incorporation of Fe_3O_4 significantly enhanced the porosity and drug loading capacity of the Mil-100(Fe) NPs, leading to a more sustained and controlled release of Flutamide under both physiological conditions and AMF exposure. The CMC hydrogel provided a biocompatible and biodegradable matrix for Flut@Mil-100(Fe) or Flut@Fe_3O_4-Mil-100(Fe) NP integration, ensuring localized drug delivery and minimizing systemic side effects. While the AMF application did not drastically alter the release kinetics from hydrogels, it slightly enhanced the release rate, suggesting potential for further optimization and hydrogel modification. Overall, this dual-functional system holds promise for improving the therapeutic efficacy of Flutamide while mitigating its adverse effects, offering a potential new avenue for targeted and personalized cancer treatment.

Future research directions for this system include several key aspects. In vivo studies should evaluate the therapeutic efficacy and safety of the developed system in animal models, focusing on tumor regression, drug distribution, and potential toxicity. Additionally, the mechanism of AMF-induced release requires further investigation to understand how AMF influences drug release from the Fe_3O_4-doped Mil-100(Fe) NPs, potentially through localized heating, magnetic force effects, or changes in nanoparticle morphology. Another important aspect is surface functionalization, where modifications such as PEGylation or the incorporation of targeting ligands could enhance nanoparticle stability, biocompatibility, and tumor-targeting efficiency. Furthermore, combination therapy should be explored to assess the potential synergistic effects of integrating this system with chemotherapy or immunotherapy, which could lead to improved treatment outcomes.

By addressing these future directions, this research can contribute to the advancement of drug delivery systems for targeted and personalized prostate cancer therapy, ultimately improving patient outcomes and quality of life.

Acknowledgment

This study received no financial support.

Authors contributions
Elham Rojouband: Project administration, Software, Writing–original draft; Saeid Mortazavinik: Methodology; Mandana Saber-Tehrani: Writing–review and editing; Maryam Bikhof: Conceptualization, Writing–review and editing; Mohammad Yousefi: Conceptualization, Supervision, Methodology.

Availability of data and materials
The data that support the findings of this study are available from the corresponding author, upon reasonable request.

Conflict of interests
The authors declare that they have no known competing financial interests or personal relationships that could have appeared to influence the work reported in this paper.

References

Aslam, S., Zeng, J., Subhan, F., Li, M., Lyu, F., Li, Y., & Yan, Z. (2017). "In situ one-step synthesis of Fe_3O_4@ MIL-100 (Fe) core-shells for adsorption of methylene blue from water". *Journal of Colloid and Interface Science*, ***505***, 186–195.

Bhattacharjee, A., Purkait, M. K., & Gumma, S. (2020). "Doxorubicin loading capacity of MIL-100 (Fe): effect of synthesis conditions". *Journal of Inorganic and Organometallic Polymers and Materials*, ***30***, 2366–2375.

Burtch, N. C., Jasuja, H., & Walton, K. S. (2014). "Water stability and adsorption in metal-organic frameworks". *Chemical Reviews*, ***114***(20), 10575–10612.

Cai, X., Bao, X., & Wu, Y. (2022). "Metal–organic frameworks as intelligent drug nanocarriers for cancer therapy ". *Pharmaceutics*, ***14***(12), 2641–2668.

Campea, M. A., Majcher, M. J., Lofts, A., & Hoare, T. (2021). "A review of design and fabrication methods for nanoparticle network hydrogels for biomedical, environmental, and industrial applications". *Advanced Functional Materials*, ***31***(33), 2102355.

Casaburi, A., Rojo, Ú. M., Cerrutti, P., Vázquez, A., & Foresti, M. L. (2018). "Carboxymethyl cellulose with tailored degree of substitution obtained from bacterial cellulose". *Food Hydrocolloids*, ***75***, 147–156.

Champion, J. A., Katare, Y. K., & Mitragotri, S. (2007). "Particle shape: A new design parameter for micro-and nanoscale drug delivery carriers". *Journal of Controlled Release*, ***121***(1-2), 3–9.

Chen, X., Tong, R., Shi, Z., Yang, B., Liu, H., Ding, S., Wang, X., Lei, Q., Wu, J., & Fang, W. (2018). "MOF nanoparticles with encapsulated autophagy inhibitor in controlled drug delivery system for antitumor". *ACS Applied Materials & Interfaces*, ***10***(3), 2328–2337.

Chen, X.-X., Hou, M.-J., Mao, G.-J., Wang, W.-X., Xu, F., Li, Y., & Li, C.-Y. (2021). "ATP-responsive near-infrared fluorescence MOF nanoprobe for the controlled release of anticancer drug". *Microchimica Acta*, ***188***(9), 287–293.

Ebrahimi, R., & Bardajee, G. R. (2021). "Sonochemical synthesis and swelling behavior of Fe_3O_4 nanocomposite based on poly (acrylamide-co-acrylic acid) hydrogel for drug delivery application". *Journal of Polymer Research*, ***28***, 35.

El-Lateef, H. M. A., Albokheet, W. A., & Gouda, M. (2020). "Carboxymethyl cellulose/metal (Fe, Cu and Ni) nanocomposites as non-precious inhibitors of C-steel corrosion in HCl solutions: synthesis, characterization, electrochemical and surface morphology studies ". *Cellulose*, ***27***, 8039–8057.

Eshrati, Y. F., Y., A. E., Yousefi, M., Far, B. F., Akbarzadeh, I., Bokov, D. O., Raahemifar, K., & Soltani, M. (2022). "Formulation and characterization of poly (ethylene glycol)-coated core-shell methionine magnetic nanoparticles as a carrier for naproxen delivery: growth inhibition of cancer cells". *Cancers*, ***14***(7), 1797.

Esmaeili, J., Barati, A., Salehi, E., & Ai, J. (2023). "Reliable kinetics for drug delivery with a microfluidic device integrated with the dialysis bag". *Molecular Pharmaceutics*, ***20***(2), 1129–1137.

Esmaeili, J., Jadbabaee, S., Far, F. M., Lukolayeh, M. E., Kırboğa, K. K., Rezaei, F. S., & Barati, A. (2022). "Decellularized Alstroemeria flower stem modified with chitosan for tissue engineering purposes: A cellulose/chitosan scaffold ". *International Journal of Biological Macromolecules*, ***204***, 321–332.

Gavilán, H., A., S. K., F.-C., T., S., N., C., M., M., B. T., C., R., & P., T. (2021). "Magnetic nanoparticles and clusters for magnetic hyperthermia: Optimizing their heat performance and developing combinatorial therapies to tackle cancer ". *Chemical Society Reviews*, ***50***(20), 11614–11667.

Ghandforoushan, P., Alehosseini, M., Golafshan, N., Castilho, M., Dolatshahi-Pirouz, A., Hanaee, J., Davaran, S., & Orive, G. (2023). "Injectable hydrogels for cartilage and bone tissue regeneration: A review". *International Journal of Biological Macromolecules*, ***246***, 125674.

Goli, P. P., Torbati, M. B., Parivar, K., Khiavi, A. A., & Yousefi, M. (2021). "Preparation and evaluation of gemcitabin and cisplatin-entrapped Folate-PEGylated liposomes as targeting co-drug delivery system in cancer therapy ". *Journal of Drug Delivery Science and Technology*, ***65***, 102756.

Hamidian, H., & Tavakoli, T. (2016). "Preparation of a new Fe_3O_4/starch-g-polyester nanocomposite hydrogel and a study on swelling and drug delivery properties ". *Carbohydrate Polymers*, ***144***, 140–148.

He, F., Zhang, M., Qian, T., & Zhao, D. (2009). "Transport of carboxymethyl cellulose stabilized iron nanoparticles in porous media: Column experiments and modeling". *Journal of Colloid and Interface Science*, ***334***(1), 96–102.

Hou, R., N., L., Du, G., Xiong, X., & F., J. (2015). "Natural polysaccharides promote chondrocyte adhesion and proliferation on magnetic nanoparticle/PVA composite hydrogels ". *Colloids and Surfaces B: Biointerfaces*, ***132***, 146–154.

Ilgin, P., Ozay, H., & Ozay, O. (2020). "Synthesis and characterization of pH responsive alginate based-hydrogels as oral drug delivery carrier". *Journal of Polymer Research*, ***27***(9), 251–265.

Javanbakht, S., Pooresmaeil, M., & Namazi, H. (2019). "Green one-pot synthesis of carboxymethylcellulose/Zn-based metal-organic framework/graphene oxide bio-nanocomposite as a nanocarrier for drug delivery system". *Carbohydrate Polymers*, ***208***, 294–301.

Karthik, R., Govindasamy, M., Chen, S.-M., Chen, T.-W., Elangovan, A., Muthuraj, V., & Yu, M.-C. (2017). "A facile graphene oxide based sensor for electrochemical detection of prostate anticancer (anti-testosterone) drug flutamide in biological samples". *Rsc Advances*, ***7***(41), 25702–25709.

Lemine, O. M. (2019). "Magnetic hyperthermia therapy using hybrid magnetic nanostructures". *Hybrid nanostructures for cancer theranostics*, *Elsevier*, 125–138.

Li, Y., Rodrigues, J., & Tomás, H. (2012). "Injectable and biodegradable hydrogels: gelation, biodegradation and biomedical applications". *Chemical Society Reviews*, ***41***(6), 2193–2221.

Londoño, D. M. M., Meyer, E., da Silva, K. J., Hernández, A. G., de Armas, R. D., Soares, L. M., Stürmer, S. L., Nodari, R. O., Soares, C. R. F. S., & Lovato, P. E. (2020). "Root colonization and arbuscular mycorrhizal fungal community composition in a genetically modified maize, its non-modified isoline, and a landrace ". *Mycorrhiza*, ***30***(5), 611–621.

Manescu, V., & P., G. (2021). "Iulian Antoniac, and Marius Vasilescu, Magnetic nanoparticles used in oncology". *Materials*, ***14***(20), 5948–5985.

Norouzi, M., Nazari, B., & Miller, D. W. (2016). "Injectable hydrogel-based drug delivery systems for local cancer therapy". *Drug Discovery Today*, ***21***(11), 1835–1849.

Olad, A., Zebhi, H., Salari, D., Mirmohseni, A., & Reyhanitabar, A. (2018). "Synthesis, characterization, and swelling kinetic study of porous superabsorbent hydrogel nanocomposite based on sulfonated carboxymethylcellulose and silica nanoparticles". *Journal of Porous Materials*, ***25***, 1325–1335.

Olusegun, S. J., O., M., M.-P., A., Ż.-M., K., N., D., K., M., P., M., & Krysinski, P. (2023). "Synthesis and characterization of Sr^{2+} and Gd^{3+} doped magnetite nanoparticles for magnetic hyperthermia and drug delivery application". *Ceramics International*, ***49***(12), 19851–19860.

Pourmadadi, M., Rahmani, E., Shamsabadipour, A., Samadi, A., Esmaeili, J., Arshad, R., Rahdar, A., Tavangarian, F., & Pandey, S. (2023). "Novel carboxymethyl cellulose based nanocomposite: A promising biomaterial for biomedical applications". *Process Biochemistry*, ***130***, 211–226.

Qazi, T. H., Muir, V. G., & Burdick, J. A. (2022). "Methods to characterize granular hydrogel rheological properties, porosity, and cell invasion". *ACS Biomaterials Science & Engineering*, ***8***(4), 1427–1442.

Reza, A. T., & Nicoll, S. B. (2010). "Characterization of novel photocrosslinked carboxymethylcellulose hydrogels for encapsulation of nucleus pulposus cells ". *Acta Biomaterialia*, ***6***(1), 179–186.

Schaeffer, E. M., Srinivas, S., Adra, N., An, Y., Barocas, D., Bitting, R., Bryce, A., et al. (2023). "Prostate cancer, version 4.2023, NCCN clinical practice guidelines in oncology". *Journal of the National Comprehensive Cancer Network*, ***21***(10), 1067–1096.

Sethi, S., Kaith, B. S., & Kumar, V. (2019). "Fabrication and characterization of microwave assisted carboxymethyl cellulose-gelatin silver nanoparticles imbibed hydrogel: Its evaluation as dye degradation ". *Reactive and Functional Polymers*, ***142***, 134–146.

Shah, R., Saha, N., Kuceková, Z., Humpolicek, P., & Saha, P. (2016). "Properties of biomineralized ($CaCO_3$) PVP-CMC hydrogel with reference to its cytotoxicity ". *International Journal of Polymeric Materials and Polymeric Biomaterials*, ***65***(12), 619–628.

Smagina, V., Yudaev, P., Kuskov, A., & Chistyakov, E. (2023). "Polymeric gel systems cytotoxicity and drug release as key features for their effective application in various fields of addressed pharmaceuticals delivery ". *Pharmaceutics*, ***15***(3), 830.

Sun, X., Gao, G., Yan, D., & Feng, C. (2017). "Synthesis and electrochemical properties of Fe_3O_4@ MOF core-shell microspheres as an anode for lithium ion battery application". *Applied Surface Science*, ***405***, 52–59.

Thang, N. H., Chien, T. B., & Cuong, D. X. (2023). "Polymer-Based Hydrogels Applied in Drug Delivery: An Overview ". *Gels*, ***9***, 523.

Tuan, M., Al-Zahara, N. F., Halim, A. H. A., & Zainuddin, N. (2021). "Carboxymethyl cellulose hydrogel from biomass waste of oil palm empty fruit bunch using calcium chloride as crosslinking agent ". *Polymers*, ***13***(23), 4056.

Uva, M., Mencuccini, L., Atrei, A., Innocenti, C., Fantechi, E., Sangregorio, C., Maglio, M., Fini, M., & Barbucci, R. (2015). "On the mechanism of drug release from polysaccharide hydrogels cross-linked with magnetite nanoparticles by applying alternating magnetic fields: the case of DOXO delivery ". *Gels*, ***1***(1), 24–43.

Wang, S., McGuirk, C. M., d'Aquino, A., Mason, J. A., & Mirkin, C. A. (2018). "Metal–organic framework nanoparticles". *Advanced Materials*, ***30***(37), 1800202.

Wu, Z., Zhang, P., Zhang, H., Li, X., He, Y., Qin, P., & Yang, C. (2022). "Tough porous nanocomposite hydrogel for water treatment ". *Journal of Hazardous Materials*, ***421***, 126754.

Xue, W., Liu, X.-L., Ma, H., Xie, W., Huang, S., Wen, H., Jing, G., Zhao, L., Liang, X.-J., & Fan, H. M. (2018). "AMF responsive DOX-loaded magnetic microspheres: transmembrane drug release mechanism and multimodality postsurgical treatment of breast cancer". *Journal of Materials Chemistry B*, ***6***(15), 2289–2303.

Zhao, D., Zhang, W., Yu, S., Xia, S.-L., Liu, Y.-N., & Yang, G.-J. (2022). "Application of MOF-based nanotherapeutics in light-mediated cancer diagnosis and therapy". *Journal of Nanobiotechnology*, ***20***(1), 421.

Zheng, H., Zhang, Y., Liu, L., Wan, W., Guo, P., Nystrom, A. M., & Zou, X. (2016). "One-pot synthesis of metal–organic frameworks with encapsulated target molecules and their applications for controlled drug delivery". *Journal of the American Chemical Society*, ***138***(3), 962–968.